Article

Valorization of Acid Mine Drainage into an Iron Catalyst to Initiate the Solar Photo-Fenton Treatment of Municipal Wastewater

Tooba Aslam [1], Vhahangwele Masindi [2,3] ⓘ**, Abdulbari A. Ahmad [1] and Efthalia Chatzisymeon [1,***

[1] School of Engineering, Institute for Infrastructure and Environment, University of Edinburgh, Edinburgh EH9 3JL, UK; tooba.aslam@ed.ac.uk (T.A.); abdulbari.saeed@ed.ac.uk (A.A.A.)
[2] Magalies Water, Scientific Services, Research & Development Division, Erf 3475, Stoffberg Street, Brits 0250, South Africa; masindivhahangwele@gmail.com
[3] Department of Environmental Sciences, College of Agriculture and Environmental Sciences, University of South Africa (UNISA), Florida 1710, South Africa
[*] Correspondence: e.chatzisymeon@ed.ac.uk; Tel.: +44-1316505711

Abstract: Acid mine drainage was utilized to catalyze the solar photo-Fenton treatment of wastewater coming from a sludge dewatering system. Acid mine drainage in the form of iron-rich liquid or synthesized minerals (namely magnetite, hematite, and goethite) was added in the wastewater, which was treated by means of the solar photo-Fenton process. The effects of operational parameters such as the amount of acid mine drainage, the wastewater matrix (i.e., synthetic and real wastewater), and the initial H_2O_2 concentration municipal wastewater's organic content were explored. The results showed that using acid mine drainage (liquid phase) for wastewater treatment was more efficient than using the acid-mine-drainage-recovered minerals. Moreover, it was observed that the addition of acid mine drainage above 10.7 mL/L wastewater, which is equivalent to 50 mg/L iron, could substantially reduce the removal percentage of the chemical oxygen demand (COD). At the best conditions assayed, COD removal reached 99% after 90 min of photo-Fenton treatment under simulated solar light, in the presence of 30 mg/L Fe (i.e., 6.4 mL drainage/L of real wastewater) and 1000 mg/L H_2O_2 at a pH of 2.8. Therefore, the solar photo-Fenton treatment of municipal wastewater catalyzed by acid mine drainage may appear to be a promising method to effectively improve wastewater management, especially in areas with high solar energy potential.

Keywords: sewage treatment; wastewater management; advanced oxidation processes; solar process; circular economy in wastewater; acid mine drainage

1. Introduction

The release of unprocessed acid mine drainage (AMD) can be a major environmental problem in countries with mining activities. AMD is the discharge of harmful substances such as heavy metals and dissolved organics coming from the reaction of water with mining waste [1]. Upon exposure to such waters, chemicals present in AMD can pose a serious threat to aquatic and terrestrial organisms [2,3]. Generally, in active mines, AMD generation can largely be avoided by using engineering solutions or in situ treatment. However, in abandoned mines, AMD can still contaminate adjacent ecosystems and receiving water bodies, as it can travel with groundwater [4–6]. Nonetheless, if AMD is managed properly, such hazards can be avoided and mitigated [4]. The conventional neutralization process for AMD treatment is still widely used, although 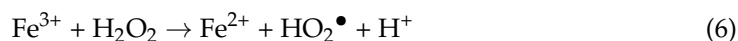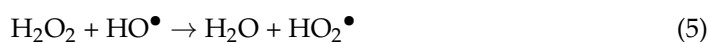it can be too complex and expensive and cause secondary contamination [7,8]. Therefore, other more sustainable treatment and management methods have recently been explored.

AMD can be an excellent resource for material recovery due to its high content of valuable metals and minerals [9]. Masindi et al. (2020) could successfully recover gypsum,

as well as Fe-species, for the production of magnetite, goethite, and hematite from real-coal-mine AMD [10]. Other substances recovered from AMD are rare earth elements and copper [11–13]. The use of iron particles recovered from AMD as adsorbents for the removal of pollutants from wastewater and for manufacturing catalysts for Fenton reactions has been previously reported [8]. Nevertheless, the synthesis of the majority of iron oxide nanoparticles takes place at high pH values and temperatures, thus increasing the complexity and the cost of the treatment.

Photo-Fenton treatment is an advanced oxidation process (AOP), which is primarily based on the generation and utilization of short-lived highly reactive radical species, such as hydroxyl radicals, $HO^{\bullet}$ (E°: 2.80 V) [6]. In the presence of solar light (solar/Fe^{2+}/H_2O_2), a renewable source of energy, additional hydroxyl radicals can be generated, as shown in Equations (1)–(11) below. These radicals can react with organic pollutants and eventually oxidize them into mineral end products such as CO_2 and water [14–19].

$$H_2O_2 + h\nu \rightarrow 2HO^{\bullet} \tag{1}$$

$$Fe^{3+} + H_2O + h\nu \rightarrow Fe^{2+} + H^+ + HO^{\bullet} \tag{2}$$

$$Fe^{2+} + H_2O_2 \rightarrow Fe^{3+} + HO^- + HO^{\bullet} \tag{3}$$

$$Fe^{2+} + HO^{\bullet} \rightarrow Fe^{3+} + HO^- \tag{4}$$

$$H_2O_2 + HO^{\bullet} \rightarrow H_2O + HO_2^{\bullet} \tag{5}$$

$$Fe^{3+} + H_2O_2 \rightarrow Fe^{2+} + HO_2^{\bullet} + H^+ \tag{6}$$

$$Fe^{3+} + HO_2^{\bullet} \rightarrow Fe^{2+} + H^+ + O_2 \tag{7}$$

$$Fe^{2+} + HO_2^{\bullet} \rightarrow Fe^{3+} + HO_2^- \tag{8}$$

$$2HO^{\bullet} \rightarrow H_2O_2 \tag{9}$$

$$2HO_2^{\bullet} \rightarrow H_2O_2 + O_2 \tag{10}$$

$$HO^{\bullet} + HO_2^{\bullet} \rightarrow H_2O + O_2 \tag{11}$$
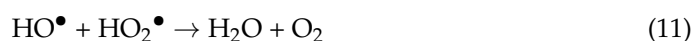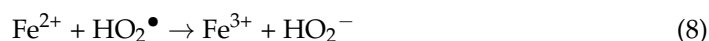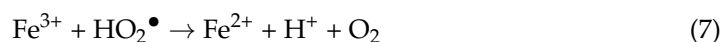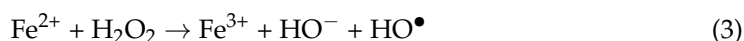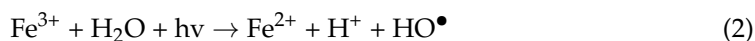
The transition of Fe^{3+} to Fe^{2+} takes place faster under solar irradiation than in dark Fenton reactions [20]. This could make solar photo-Fenton process an attractive option for mitigating water pollution, especially in locations such as South Africa, where solar irradiation is abundant [21] and access to clean water may not always be presumed. Moreover, Fenton reactions take place in an acidic environment (optimal pH is 2.8), which makes it an even more attractive process for the management of AMD, which is a highly acidic substance (pH can range from 2 to 4) [9].

Many studies have focused on the use of iron-rich AMD sludge to remove pollutants from water. For example, Tony et al. (2022) utilized AMD sludge as a source of iron to start Fenton reactions and developed a lab-scale system, which achieved a 73% COD decrease at an optimum AMD sludge concentration of 41 mg/L. Moreover, a 91.4% removal of organics from vehicle-washing water was achieved at a pH of 4.0, using 92 mg/L and 354 mg/L of AMD sludge and H_2O_2 concentrations, respectively [22]. To the best of our knowledge, there is no study that has explicitly dealt with utilization of AMD effluent (i.e., liquid phase and not the sludge) for the degradation of pollutants in a photo-Fenton treatment system. It should be noted that the co-treatment of AMD effluent and municipal wastewater has been previously studied by our group [23] by means of dilution, precipitation, co-precipitation, adsorption, and crystallization processes. In that study, it was observed that, due to the

AMD's high iron content, the addition of a Fenton-based step in the co-treatment train system could potentially enhance its feasibility.

Therefore, the aim of this study was to use an AMD effluent as a source of iron to catalyze the treatment of municipal wastewater (MWW) in a solar photo-Fenton system. Operational parameters such as the iron and H_2O_2 concentration, the organic content of the wastewater, and the water matrix (i.e., synthetic and real wastewater) were explored. AMD-recovered iron-rich catalysts were also tested and compared to using an AMD effluent in the treatment process. The results could be used to develop a sustainable treatment system based on the use of solar energy that would work in a circular economy manner, where waste from one source (i.e., AMD) is used as a resource for the treatment of another waste (i.e., MWW).

2. Materials and Methods

2.1. Materials

The synthetic wastewater (Table 1) was prepared by using $FeSO_4.7H_2O$ (CAS No. 7782-63-0; $\geq$99.0%), $NaO_2C_2H_3$ (CAS No. 6131-90-4; $\geq$99%), K_2HPO_4 (CAS No. 7758-11-4; $\geq$98%), and $CaCl_2$ (CAS No. 10035-04-8; $\geq$99%) purchased from Sigma Aldrich (Dorset, UK). $MgSO_4.7H_2O$ (CAS No. 10034-99-8; 99.5%) from Fisher Scientific and NH_4Cl (CAS No. 12125-02-9; $\geq$99.5%) from Sigma Life Science were also used as received. H_2O_2 (CAS No. 7722-84-1; 35%), which was purchased from Sigma Aldrich (Dorset, UK), was used as an additional oxidant.

Table 1. Chemical composition and physicochemical characteristics of synthetic wastewater.

Synthetic Wastewater (SWW)			
Composition		**Physicochemical Characteristics**	
Chemical Compound	**Concentration (mg/L)**	**Property**	**Value**
$C_2H_9NaO_5$	1500	pH	7.08
NH_4Cl	400	COD	768 mg/L
K_2HPO_4	21		
$FeSO_4.7H_2O$	10		
$MgSO_4.7H_2O$	12		
$CaCl_2.2H_2O$	14		

Real wastewater was collected from a sludge dewatering stream at a municipal wastewater treatment plant in Gauteng Province in South Africa, and its physicochemical characteristics are shown in Table 2. Wastewater samples were stored in high-density polyethylene narrow-mouthed closed-top bottles and were kept at 4 °C. Instantly after collection, the wastewater dewatering effluent was passed through a Macherey-Nagel filter paper (MN 615; 125 mm) to get rid of the suspended solids and debris. AMD was collected from an active coal mine in Mpumalanga Province (South Africa), and similarly with the municipal wastewater dewatering effluent, AMD was filtered to eradicate the suspended solids and debris. Its physicochemical characteristics are also shown in Table 2. Hematite, goethite, and magnetite were recovered from AMD based on a process described in our previous publication [10] and were used as catalysts to initiate the solar photo-Fenton treatment of municipal wastewater.

Table 2. Physicochemical characteristics of acid mine drainage and real municipal wastewater.

Property	Acid Mine Drainage (AMD)	Municipal Wastewater (MWW)
pH	2.6	12.2
COD	111 mg/L	255 mg/L
Total solids	29.19 mg/L	1.68 mg/L
Iron	4652.1 mg/L	0.03 mg/L
Calcium	562.4 mg/L	11.05 mg/L
Magnesium	481.9 mg/L	0.43 mg/L
Manganese	94.25 mg/L	0.00237 mg/L
Zinc	9.12 mg/L	0.00715 mg/L
Copper	5.98 mg/L	0.00281 mg/L
Cobalt	1.22 mg/L	0.0012 mg/L
Arsenic	-	0.00424 mg/L
Cadmium	0.02 mg/L	<0.0015 mg/L

2.2. Experimental Procedure

All experiments were carried out in a photocatalytic reactor at 150 mL working volume and at batch mode. A solar simulator (Oriel® LCS-100™; Small Area Sol1A) was used to resemble natural solar light, and irradiation was entering in the whole volume of the wastewater from the top of its surface. The UVA irradiation intensity emitted by the solar simulator was measured by a UVP UVX Radiometer (Analytik Jena, London, UK), which was 4.28 mW/cm^2 at the larger distance from the lamp, and at the very top, next to the lamp, it was 18.85 mW/cm^2. The wastewater was continuously magnetically stirred (150–200 rpm) to achieve uniform mixing and to promote dispersion. Iron was added in the wastewater either as appropriate amounts of AMD or minerals, namely hematite, goethite, and magnetite, or in the form of $FeSO_4$. After that, the pH was brought to 2.8 by using 1 M nitric acid (70% HNO_3). Once the pH was regulated, an appropriate amount of H_2O_2 was added to the wastewater. Then, the solar simulator was switched on, and the samples were periodically taken from the reactor; filtered through 0.45 μm polyvinylidene fluoride (PVDF) syringe filters (CM Scientific Ltd., Keighley, UK); and analyzed for COD, metals and H_2O_2 concentration, pH, and UV-Vis absorbance. All experiments were carried out at room temperature. In all cases, the initial pH of 2.80 for the reactant solution was slightly decreased to 2.40–2.60 after 180 min of treatment. Representative experiments were carried out in triplicates, and it was found that the standard error in COD removal was less than 5%.

2.3. Analytical Methods

2.3.1. Solid Characterization

The morphological, mapping, and elemental properties of goethite (FeO_2H), hematite (Fe_2O_3), and magnetite (Fe_3O_4) were measured using high-resolution (HR) field-emission scanning electron microscope (FE-SEM) (SmartSEM®-Auriga®, North Berwick, UK) coupled with a focused ion beam (FIB) and energy dispersive spectroscopy (EDS). Moreover, the crystallography and micro-graphical properties of goethite, hematite, and magnetite were further determined using high-resolution transmission electron microscopy (TEM) (JEOL TEM-2100 electron microscope) equipped with EDS capabilities to support SEM-EDS results. The National Institute of Standards and Technology (NIST) standards were used for quality control and calibration of the instruments, and all analyses were performed in ISO-accredited laboratories.

2.3.2. Aqueous Characterization

Photocatalytic performance was evaluated with respect to organic removal from wastewater by measuring its chemical oxygen demand (COD) according to the potassium dichromate standard method. A YSI 910 COD Colorimeter (YSI Xylem Analytics, Letchworth Garden City, UK), COD digestion tubes (Palintest PL450 (0–150 mg L^{-1}) or PL484 (0–1500 mg L^{-1})), and a block heater (Hach 16500-10) were used for COD measurements. H_2O_2 was monitored by the peroxide test strips (1–100 mg/L H_2O_2) purchased from Fisher Scientific, UK. The pH was measured by using WTW OXI340i Oxygen Meter with a compatible pH probe. A Cary 100 Scan UV-Vis Spectrophotometer (VARIAN, Crawley, UK) was used to measure wastewater's absorbance at the 254–800 nm spectrum. The Mg, P, Ca, and Fe concentrations in water were analyzed by 8900 Triple Quadrupole ICP-MS (Agilent with an octopole reaction system), employing an RF power of 1550 W and RF Matching voltage of 1.8 V, with argon gas flows of 15 L/min, 0.9 L/min, and 1.03 L/min for plasma, auxiliary, and nebulizer flows, respectively. The spectrometer was operated in single quad mode, with He gas added into the collision cell for the removal of interferents, with a He flow rate of 10 mL/min.

3. Results and Discussion

3.1. AMD-Recovered Catalyst

The morphological, microstructural, and mapping properties of goethite (FeO_2H), hematite (Fe_2O_3), and magnetite (Fe_3O_4), along with their EDS characteristics, are reported below.

3.1.1. Map Sum Spectrums

The SEM-EDS spectrums for goethite, hematite, and magnetite were determined, and their corresponding spectrums, along with the surface elemental compositions, are shown in Figure 1. As observed in Figure 1a–c, the elemental composition of all recovered and synthesized Fe-species comprised Fe, C, and O as major elements, along with traces of Mg, Ca, Si, Al, Ti, S, and Mn. The presence of O can be traced back to the fact that the synthesized minerals are Fe-hydroxide, while C can be traced back to the coating material as a substrate (fine carbon layers) used in SEM for measurements of microstructural materials and to improve the imaging of the Fe-based samples, not attributed to the mother material; hence, it was disregarded in this study. To be more specific, it was estimated that the synthesized goethite, hematite, and magnetite comprised close to 70% of the Fe content in its microstructural matrices, micelles, and interlayers, thus confirming that these are Fe-based minerals.
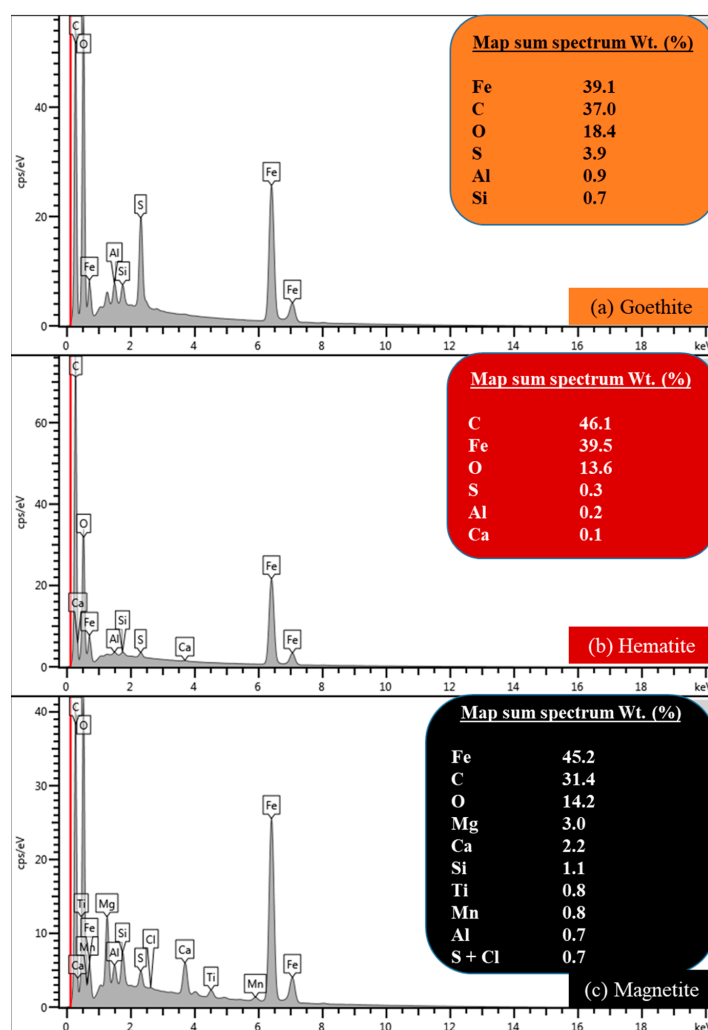
Figure 1. The elemental composition of (**a**) goethite (FeO_2H), (**b**) hematite (Fe_2O_3), and (**c**) magnetite (Fe_3O_4), using the SEM-EDS spectrums.

3.1.2. Microstructural Morphology from Transmission Electron Microscopy

The micrographs of (a) goethite (FeO_2H), (b) hematite (Fe_2O_3), and (c) magnetite (Fe_3O_4) are shown in Figure 2.
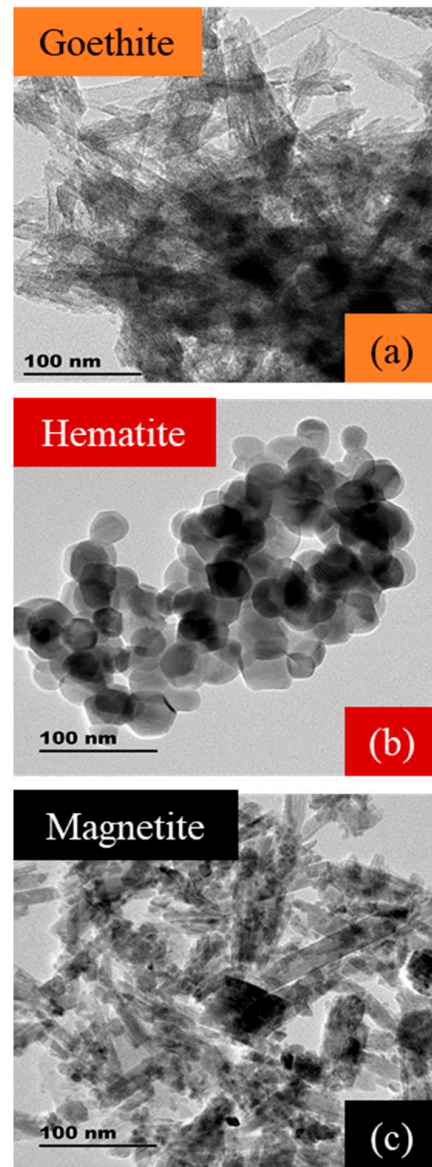
Figure 2. The HR-TEM micrographs show the morphological properties of (**a**) goethite (FeO_2H), (**b**) hematite (Fe_2O_3), and (**c**) magnetite (Fe_3O_4) at 100 nm magnification.

The results in Figure 2a–c clearly show that these materials comprise mixtures of spherical and rod-like particles nanoparticles and sheets overlapping on top of each other. To be more specific, the goethite (Figure 2a) and magnetite (Figure 2c) micrographs showed the presence of rods meshed with spherical particles, while for hematite (Figure 2b), the presence of polygonal and spherical nanosheets meshed to each other was observed. Particles were consistent on the surface of all minerals, thus confirming that the used minerals are homogeneous in terms of microstructural properties.

3.1.3. Focused Ion Beam Scanning Electron Microscopy

The morphological and microstructural characteristics of (a) goethite (FeO_2H), (b) hematite (Fe_2O_3), and (c) magnetite (Fe_3O_4) were ascertained using FIB-SEM (Figure 3a–c). In essence, advanced HR-FIB-SEM-EDS was used to acquire clear, vivid, and high-resolution images that

can meticulously depict microstructural and morphological properties. It was observed that goethite and magnetite comprised spherical and rod-like structures on their matrices, while hematite comprised spherical structures meshed together. The morphology was homogeneous in all cases. Interestingly, the obtained results were congruent with the results obtained from the HR-TEM, hence confirming the obtained results and our previous studies [9,24].
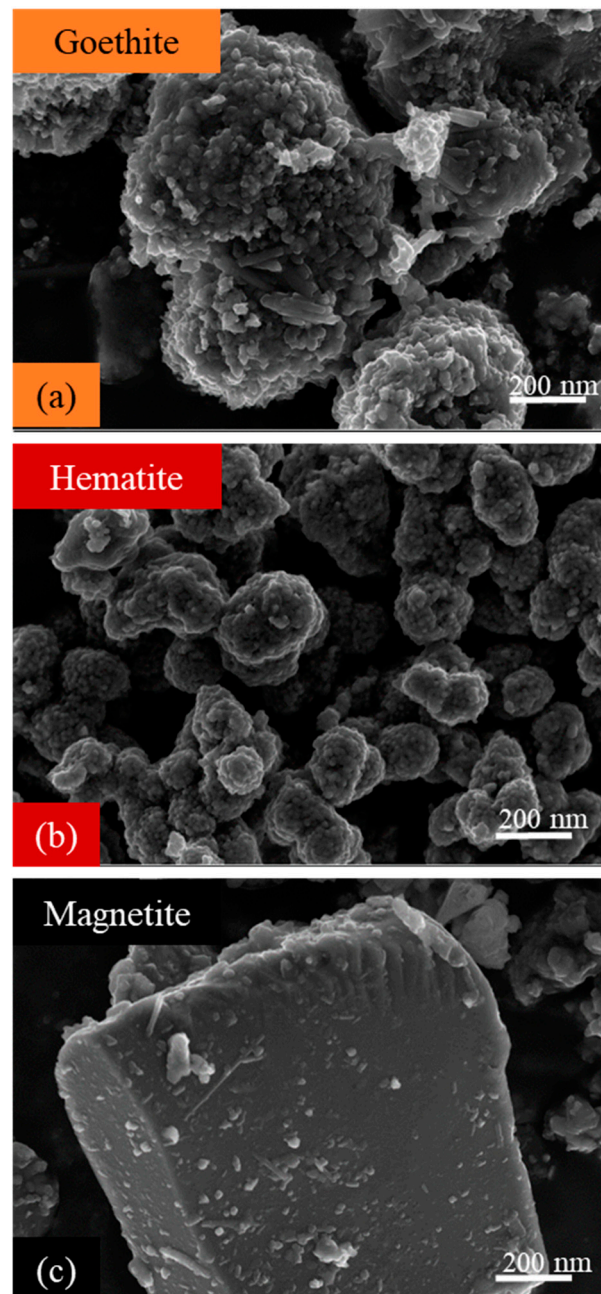
Figure 3. High-resolution FIB-SEM images showing morphological properties of (**a**) goethite (FeO_2H), (**b**) hematite (Fe_2O_3), and (**c**) magnetite (Fe_3O_4) at 200 nm magnification.

3.1.4. Mapping of Elemental Distribution Using EDS

To further corroborate the SEM-EDS results as they pertain to the elemental compositions of goethite (FeO_2H) (a–e), hematite (Fe_2O_3) (a–e), and magnetite (Fe_3O_4) (a–e), elemental distribution mapping was also appraised using the HR-FE-SEM instrument equipped with the EDS capabilities. The results are shown in Figure 4.
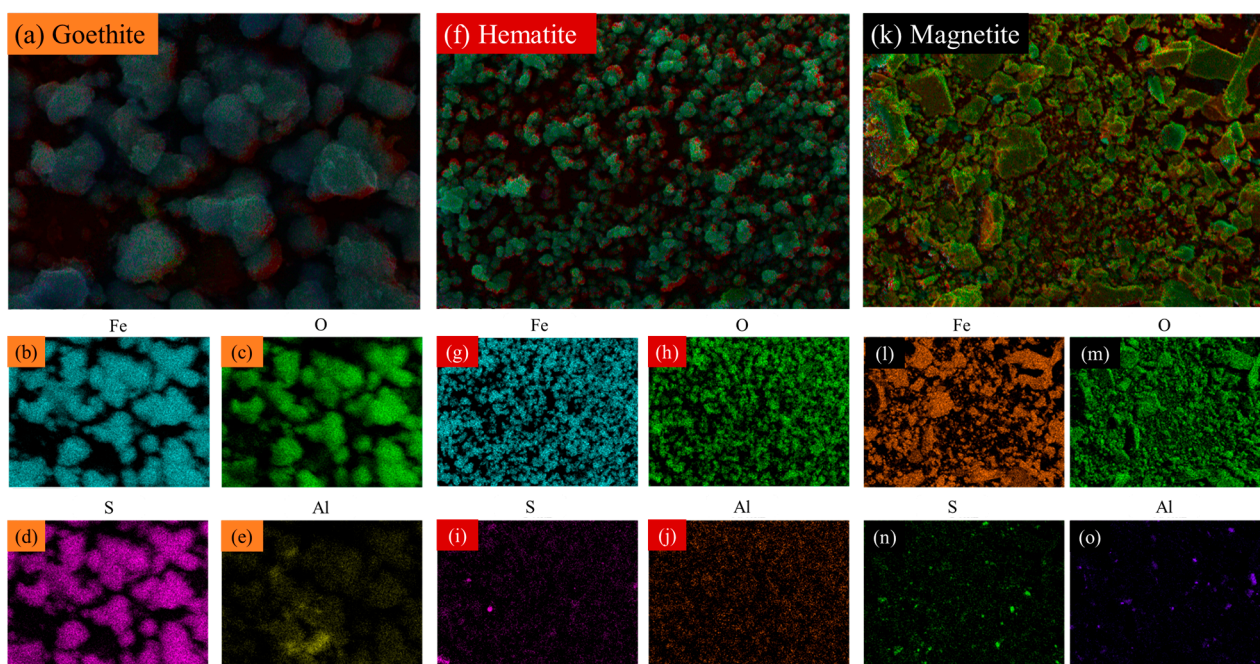
Figure 4. The SEM-EDS imagery (**a**,**f**,**k**) and elemental maps of goethite (FeO_2H) (**b**–**e**), hematite (Fe_2O_3) (**g**–**j**), and magnetite (Fe_3O_4) (**l**–**o**).

The cut-across mapping of elemental distribution on the surface of goethite, hematite, and magnetite can be shown in Figure 4. Specifically, goethite comprised Fe, O, S, and Al as principal elements. The presence of Fe and O indicates the formation of Fe hydroxide, hence the name Fe-hydroxide minerals; meanwhile, the presence of S, which precisely overlaps or is meshed to Fe and O, denotes the formation of Fe oxyhydrosulphates in goethite matrices. Moreover, it was observed that hematite comprised Fe, O, S, and Al as principal elements. Fe and O denote the presence of Fe hydroxide, while Al and S indicate that Al and Fe oxyhydrosulphates might have been formed. This is consistent with results reported in our previous studies [10,23–25]. A similar trend was also observed for magnetite.

3.2. Photo-Fenton Treatment Process Using AMD-Recovered Catalysts

In our previous publication [11], iron was recovered from AMD in the mineral forms of magnetite, hematite, and goethite. These iron-rich minerals (with $\geq 70\%$ Fe content, wt.%) were added in municipal wastewater to initiate the photo-Fenton treatment process. The results are shown in Figure 5. Control experiments in the presence of 1000 mg/L H_2O_2 in the dark and under simulated solar light, as well as under solar light alone, were also carried out. The results from these experiments showed that COD removal of the wastewater was less than 7% in all cases.

It was observed that COD removal was 35%, 25%, and 7% in the presence of hematite, goethite, and magnetite, respectively. As can be seen in Figure 5b–d the concentration of dissolved Fe in water was 10 mg/L for hematite and goethite but only 1 mg/L for magnetite. These relatively higher iron concentrations were probably the reason why hematite and goethite yielded higher COD removal efficiency than magnetite. This is also consistent with chemical reactions (2) and (3), which show that increased amounts of iron, such as in hematite and goethite, can increase the production of hydroxyl radicals thus oxidizing the pollutants at higher rates. Moreover, results showed that the amount of total iron in water was reduced after the end of treatment by about 40%, 10%, and 15% for goethite, hematite, and magnetite, respectively. This may be attributed to the fact that small amounts of iron might have precipitated in the form of Fe^{3+} in the solution during photo-Fenton oxidation. As far as the other metals are concerned, Mg, Ca, and P remained almost unchanged during treatment in the presence of hematite and goethite, while for magnetite, their concentration slightly

increased at the end of treatment. Moreover, it should be noted that the initial 1000 mg/L H_2O_2 was consumed in the first 30 min of treatment, reaching a plateau of 100 mg/L H_2O_2, which remained almost constant until the end of the treatment (i.e., 180 min). This indicates that chemical reactions (1) and (3) were favored in the first 30 min of treatment and after that radicals were generated mainly by means of chemical reaction (2), since no further considerable H_2O_2 consumption was observed.
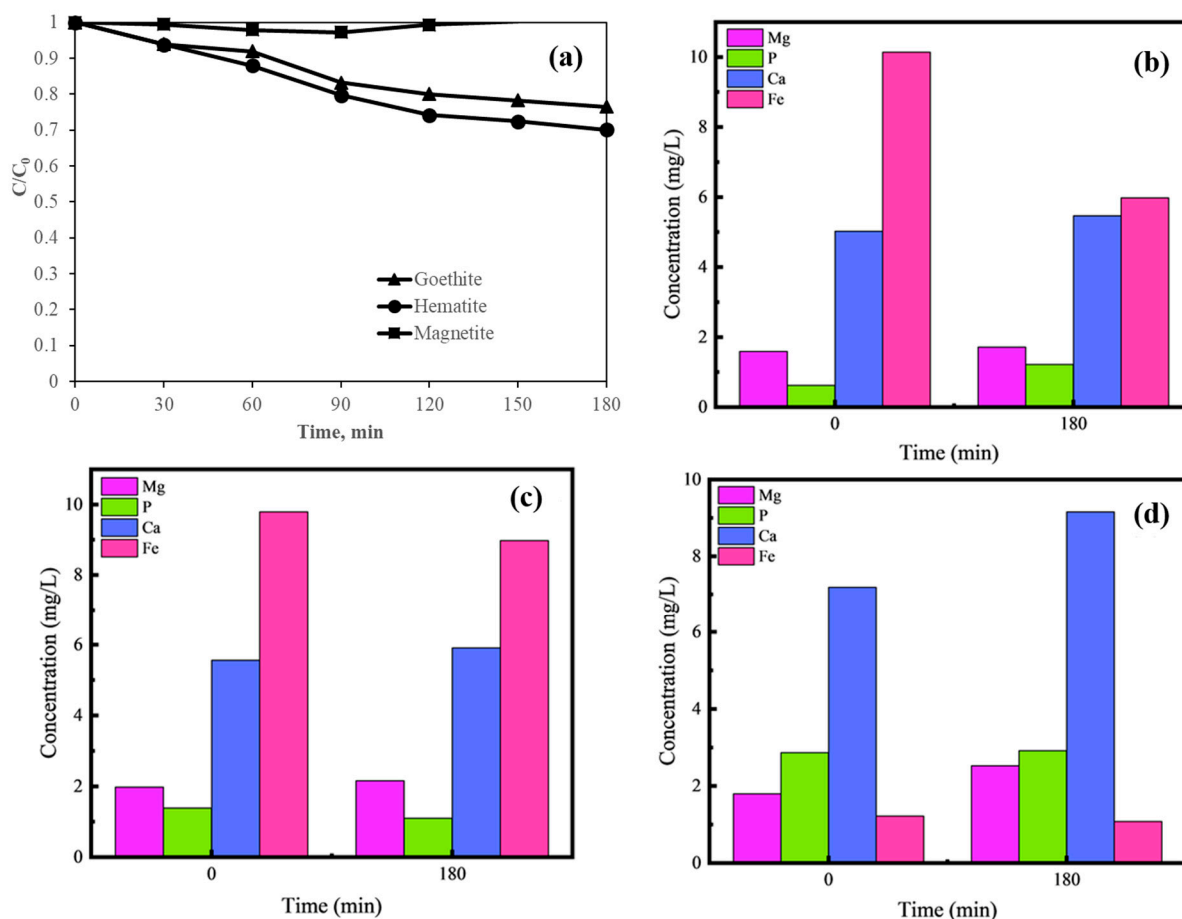
Figure 5. (**a**) COD removal in the presence of AMD-recovered catalysts during solar photo-Fenton treatment. Metal concentration in water before and after 180 min treatment in the presence of (**b**) goethite, (**c**) hematite, and (**d**) magnetite. Experimental conditions: SWW; 1000 mg/L H_2O_2; initial pH is 2.8; catalyst concentration is 1 g/L; influent COD = 725 ± 20 mg/L.

To further explore the COD removal potential of hematite and goethite in the solar photo-Fenton process, more experiments were carried out at catalyst concentrations of 1 g/L, 2 g/L, and 4 g/L (Figure 6). It was observed (Figure 6a) that COD was 30%, 29%, and 23% removed in the presence of 1 g/L, 2 g/L, and 4 g/L of hematite, respectively, showing that, by increasing hematite's initial concentration, the COD removal rates start to slightly decrease. Similarly, COD removal was 24%, 11%, and 12% in the presence of goethite concentrations of 1 g/L, 2 g/L, and 4 g/L, respectively (Figure 6b). It can be observed that when the goethite concentration is doubled from 1 g/L to 2 g/L, the COD removal is more than halved (from 24% to 11%). This decline in COD removal, which was observed for both hematite and goethite, might be attributed to the fact that (a) high amounts of catalyst (e.g., 2 g/L and 4 g/L) can hinder the penetration of solar light into the bulk solution by absorbing, scattering, or reflecting irradiation; and (b) the catalyst's high amounts of suspended particles can shield organic pollutants, thus inhibiting oxidation. Catalyst concentrations at the same order, such as 0.75 g/L [26], 1 g/L [27], and 3 g/L [28], have

been previously reported as optimal for solar heterogeneous photocatalysis of municipal, colored, and agro-industrial wastewater, respectively.
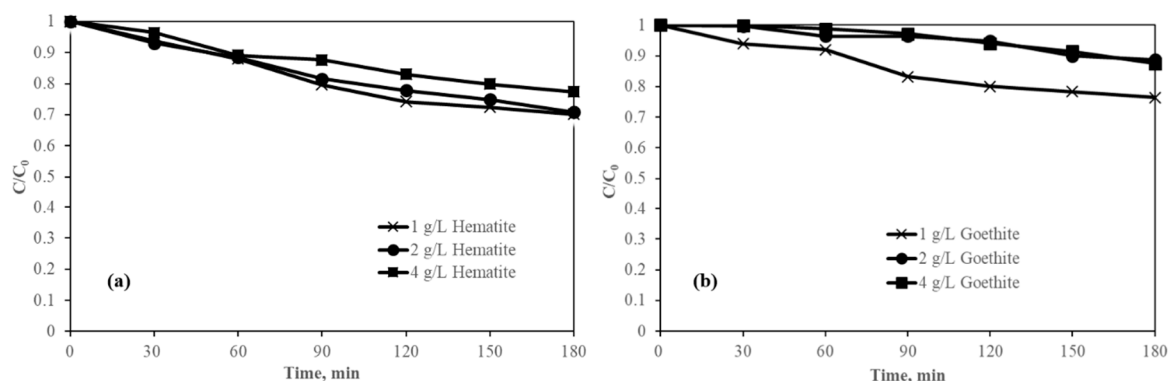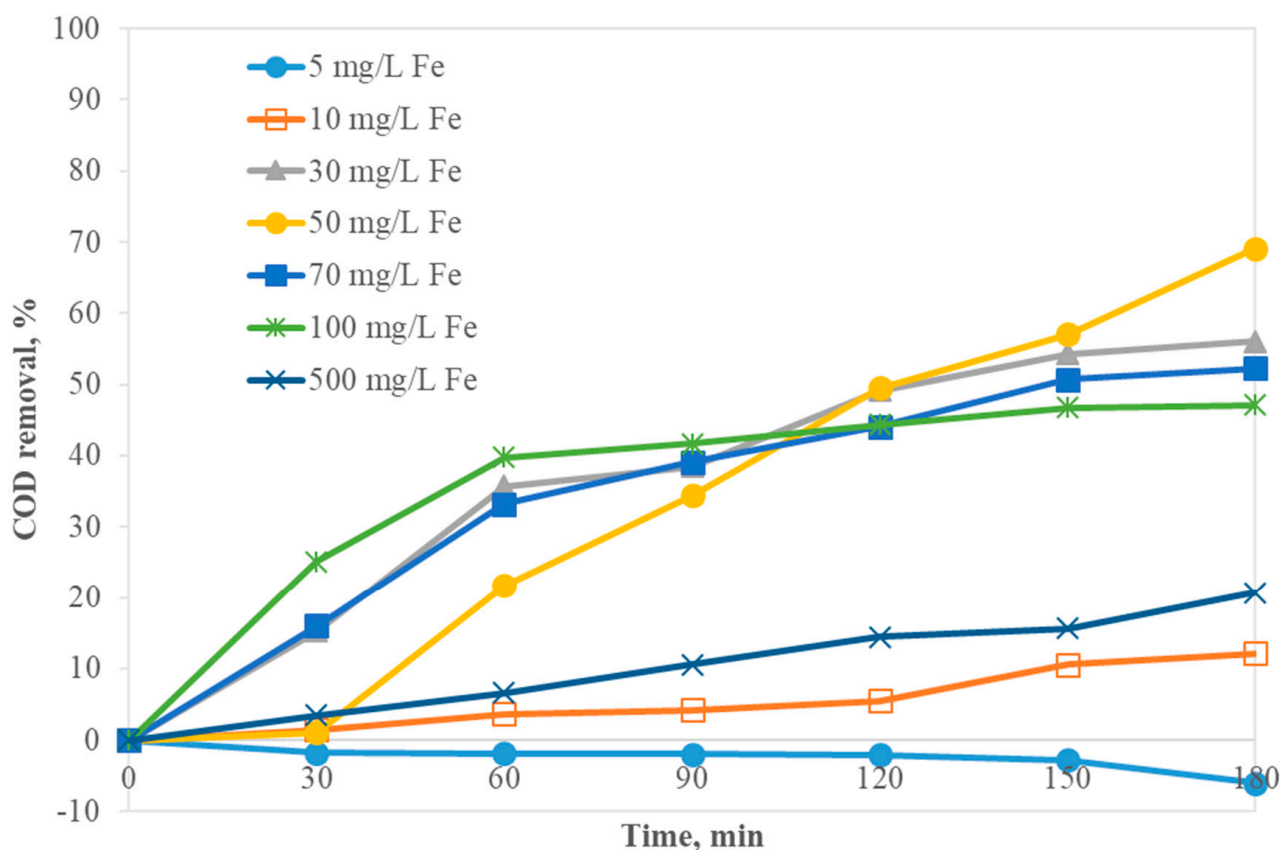

Figure 6. COD removal in the presence of various concentrations of (**a**) hematite and (**b**) goethite. Experimental conditions: SWW; 1000 mg/L H_2O_2; pH is 2.8.

3.3. AMD Catalyzed Photo-Fenton Reaction

To assess whether the addition of AMD (liquid phase) can achieve higher COD removal rates than those yielded in the presence of AMD recovered minerals, as was described in the previous section, the following experiments (Figure 7) were carried out. First, 161×10^{-3} mL (1.1 µL ADM/mL SWW), 322×10^{-3} mL (2.1 mL ADM/L SWW), 967×10^{-3} mL (6.4 mL ADM/L SWW), 1612×10^{-3} mL (10.7 mL ADM/L SWW), 2257×10^{-3} mL (15 mL ADM/L SWW), and 3224×10^{-3} mL (21.5 mL ADM/L SWW) AMD were added to 150 mL synthetic wastewater, matching with the initial Fe concentrations (as measured by ICP-OES) of 5 mg/L, 10 mg/L, 30 mg/L, 50 mg/L, 70 mg/L, and 100 mg/L, respectively. The results showed that COD removal increases to 12%, 56%, and 69% in the presence of 10, 30 and 50 mg/L iron, respectively, during the co-treatment of wastewater with appropriate amounts of AMD. These results can be attributed to the fact that, at low iron concentrations (e.g., ≤10 mg/L), the amount of $HO^{\bullet}$ and other reactive species generated in the water is low, and only some of the organics are oxidized. Figure 7 shows that an increase in iron at 30 mg/L and 50 mg/L is sufficient to degrade 56% and 69% COD, respectively. Above this point, it was observed that COD removal decreases at 52%, 47%, and 20% (in the presence of 70, 100, and 500 mg/L iron), respectively. This decline in photo-Fenton efficiency at concentrations ≥50 mg/L Fe could be attributed to increased amounts of Fe^{2+}/Fe^{3+} in the solution, which can form chromophoric complexes with organic matter in water [28] and/or can scavenge hydroxyl radicals, as described in Equation (4). Iron can be found in AMD in both Fe^{2+} and Fe^{3+} forms, with the latter tending to precipitate in water due to its relatively low solubility. The presence of chromophores was indicated by an increase in UV-Vis absorbance in the visible area of the spectrum. For example, at 400 nm, the initial UV-Vis absorbance was 0.123, 0.143, 0.214, and 0.814 with 5 mg/L, 10 mg/L, 50 mg/L, and 100 mg/L Fe. These chromophores could absorb the irradiation emitted from the solar simulator, therefore decreasing the photon energy available for organics oxidation and the removal of COD from water. Moreover, Fe^{3+} might be possible to precipitate in the water, even at trace concentrations, despite its low pH. The presence of these solid particles in the solution may have also contributed, to a much lesser extent than chromophores, to the decrease in COD removal. It has been previously reported that, at a pH of 2, the oxidation rate of 100 mg/L Fe^{2+} into Fe^{3+} was 8.4×10^{-7} µg/L, which, in addition to the 29.19 mg/L of solids already contained in AMD, may have contributed to the decreasing COD removal. This could be attributed to the fact that the penetration of irradiation into the whole water volume can be prevented due to light reflection, refraction, or scattering processes. Moreover, increased amounts of solids in water might shade organic pollutants from light and inhibit their oxidation. Therefore,

the optimal process efficiency can be obtained in the presence of 50 mg/L Fe sourced from AMD.

Figure 7. COD removal during treatment of wastewater with AMD at appropriate amounts to yield iron at various concentrations, ranging from 5 mg/L to 500 mg/L. Experimental conditions: SWW; 1000 mg/L H_2O_2; pH is 2.8; simulated solar light.

3.4. Effect of H_2O_2 Concentration

Several H_2O_2 concentrations in the range of 100–1000 mg/L were tested to explore its effect on the photo-Fenton wastewater treatment catalyzed by AMD. Figure 8 shows that COD removal was 25%, 30%, 34%, 40%, and 50% after 180 min of treatment in the presence of 100 mg/L, 200 mg/L, 400 mg/L, 800 mg/L, and 1000 mg/L H_2O_2. It was observed that COD removal increases when the initial H_2O_2 is increased, which can be attributed to the increase in $HO^\bullet$ radicals generated in water due to the photo-Fenton decomposition of H_2O_2, as described in chemical reactions (1) and (3). This is consistent with H_2O_2 measurements, which showed (data not presented) that H_2O_2 was consumed after about 150 min of treatment, in almost all cases, when COD removal percentages practically reached a plateau with no further increase. Therefore, subsequent experiments were carried out at 1000 mg/L H_2O_2, as it was deemed that a further increase in the H_2O_2 amount would impact the environmental sustainability and cost of the process.
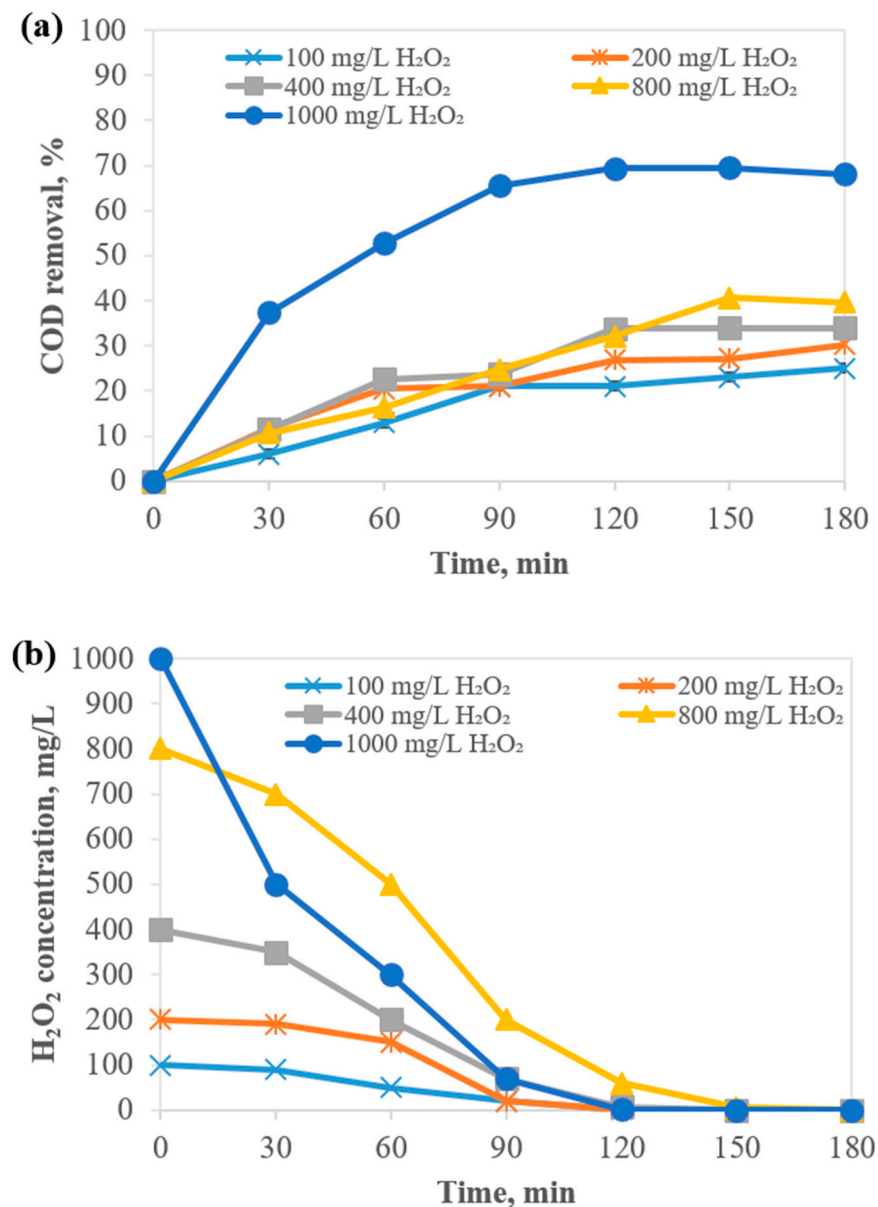
Figure 8. (**a**) COD removal and (**b**) hydrogen peroxide concentration during photo-Fenton treatment of synthetic wastewater (SWW) in the presence of different initial concentrations of H_2O_2. Experimental conditions: 5 mg/L $FeSO_4$; pH is 2.8.

3.5. Effect of Influent's Organic Content

A common technical challenge in wastewater engineering is that the physicochemical characteristics of wastewater, including its organic content, can vary significantly between sampling times. Assessing the kinetic reaction rates could adequately address this issue. Therefore, experiments were carried out at different initial COD concentrations (205 mg/L, 391 mg/L, and 739 mg/L) by diluting synthetic wastewater with appropriate amounts of de-ionized water (i.e., SWW:DW ratios were 1:4, 1:2, and 1:1, respectively). The results are shown in Figure 9, where it can be observed that the COD removal was 25%, 36%, and 54% after 180 min of treatment for wastewater with an initial COD of 739 mg/L, 391 mg/L, and 205 mg/L, respectively.
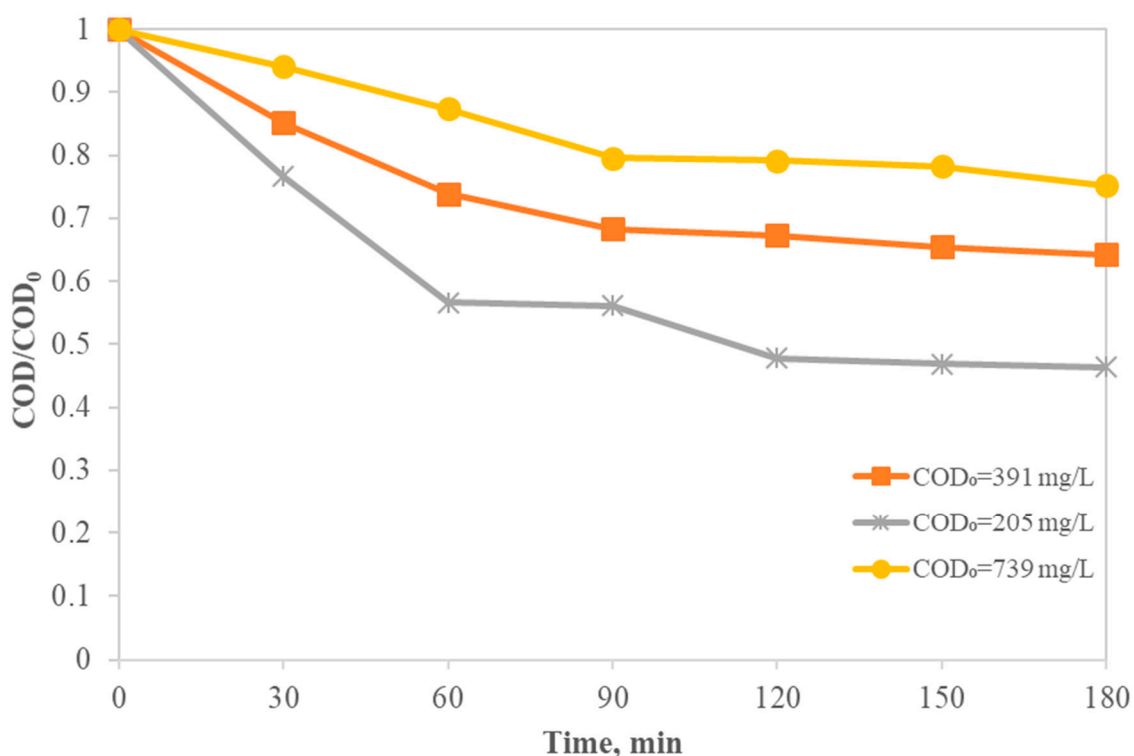
Figure 9. COD removal in the presence of different initial COD concentrations of wastewater. Experimental conditions: SWW; 100 mg/L H_2O_2; 5 mg/L $FeSO_4$; initial pH is 2.8.

This increase in process efficiency when the initial organic content decreased could be attributed to the fact that, at a low initial COD, there were lower amounts of organic pollutants in the water, and therefore, a greater amount of them can be oxidized by the available oxidative species generated during the process. Moreover, it was observed that the reaction rate fit better into a pseudo-first-order reaction model with degradation rates remaining almost unchanged at 0.05 min^{-1} and 0.07 min^{-1} for an initial of COD 739 mg/L and 391 mg/L and slightly increased to 0.12 min^{-1} when the initial COD was 205 mg/L.

3.6. Treatment of Real Municipal Wastewater Catalyzed by AMD

Appropriate amounts of AMD were added in real municipal wastewater so that the influent mixture contained 5 mg/L, 30 mg/L, and 50 mg/L of iron. Experiments were carried out in triplicates, and it was found that the standard error in COD removal was less than 5%. The results (Figure 10) showed that COD removal reached 26%, 99%, and 78% after only 90 min of treatment in the presence of 5 mg/L, 30 mg/L, and 50 mg/L Fe sourced from AMD, respectively. Nevertheless, achieving almost complete decontamination in the presence of 30 mg/L Fe (i.e., 6.4 mL ADM/L MWW) after 90 min of photo-Fenton treatment under solar irradiation constitutes this a promising process for larger-scale applications. Furthermore, it was observed that the removal percentages are higher for co-treating AMD with MWW than in the case of SWW, and this outcome could be explained by the different initial COD content of the two types of matrices. To be more specific, the organic content of SWW with an initial COD 700 mg/L needs more time to be oxidized than MWW with an initial COD of 270 mg/L, which is consistent with results shown in Figure 9. This difference is apparent in Figure 10, where experiments with SWW and MWW are shown for the sake of comparison.
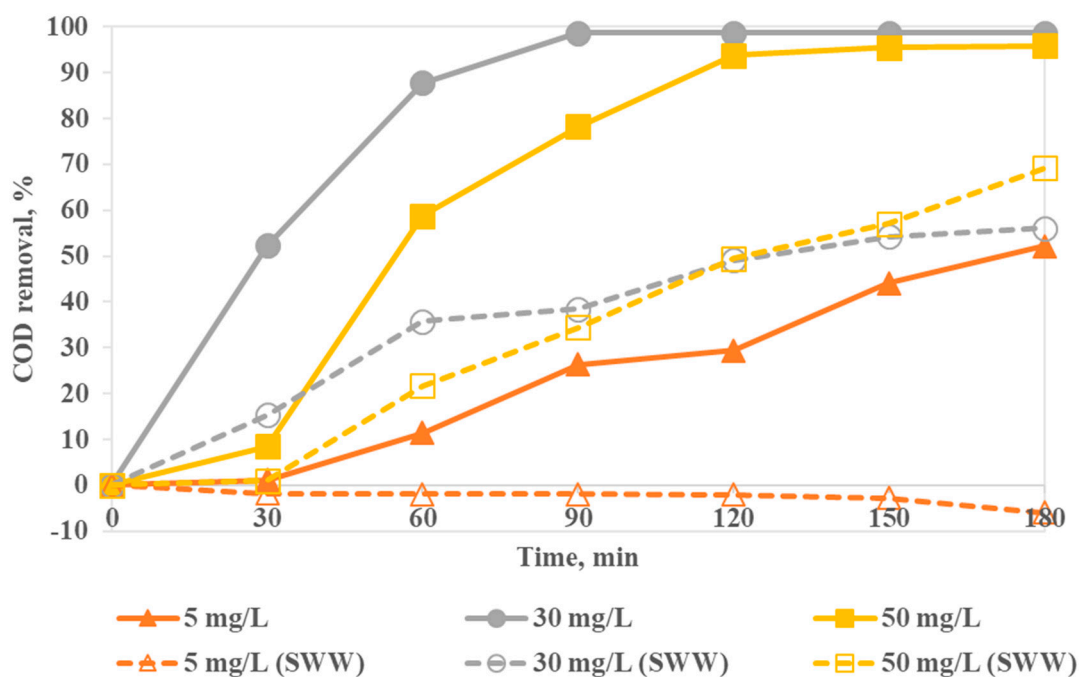
Figure 10. COD removal after solar photo-Fenton treatment of municipal wastewater (MWW) catalyzed by AMD at appropriate amounts to yield 5 mg/L, 30 mg/L, and 50 mg/L Fe in the influent mixture. Dash lines show the experiments (also shown in Figure 7) carried out with synthetic wastewater (SWW). Experimental conditions: 1000 mg/L H_2O_2; pH is 2.8.

4. Conclusions

Iron-rich acid mine drainage (AMD) was used as a source of iron to treat wastewater from a sludge dewatering system via the solar photo-Fenton process to promote a circular economy in wastewater management. Minerals recovered from AMD were synthesized and tested as catalysts for the photo-Fenton treatment. Moreover, to the best of the authors' knowledge, this is the first time that AMD (liquid phase) was used as a catalyst for the solar photo-Fenton treatment of wastewater. It was observed that process efficiency in terms of COD removal is higher when AMD is directly added into the wastewater rather than in the form of AMD-recovered catalysts, namely magnetite, hematite, and goethite. The effect of operational parameters such as the influent's organic content, catalyst concentration, and iron and hydrogen peroxide concentration was studied. At the best conditions essayed, almost complete decontamination could be achieved, thus rendering the proposed method a promising sustainable technique for wastewater management, especially in areas with high solar energy potential.

References

1. Masindi, V.; Akinwekomi, V.; Maree, J.; Muedi, K. Comparison of mine water neutralisation efficiencies of different alkaline generating agents. *J. Environ. Chem. Eng.* **2017**, *5*, 3903–3913. [CrossRef]
2. Seo, J.; Kwon, D.; Yoon, T.H.; Jung, J. Potential risks of the natural nanoparticles from the acid mine drainage and a novel approach for their toxicity assessment. *Toxicol. Environ. Health Sci.* **2010**, *2*, 215–220. [CrossRef]
3. Talukdar, B.; Kalita, H.; Baishya, R.; Basumatary, S.; Sarma, D. Evaluation of genetic toxicity caused by acid mine drainage of coal mines on fish fauna of Simsang River, Garohills, Meghalaya, India. *Ecotoxicol. Environ. Saf.* **2016**, *131*, 65–71. [CrossRef] [PubMed]
4. Masindi, V.; Osman, M.S.; Shingwenyana, R. Valorization of acid mine drainage (AMD): A simplified approach to reclaim drinking water and synthesize valuable minerals—Pilot study. *J. Environ. Chem. Eng.* **2019**, *7*, 103082. [CrossRef]
5. Wang, Z.; Xu, Y.; Zhang, Z.; Zhang, Y. Review: Acid Mine Drainage (AMD) in Abandoned Coal Mines of Shanxi, China. *Water* **2021**, *13*, 8. [CrossRef]
6. Armstrong, D.A.; Huie, R.E.; Lymar, S.; Koppenol, W.H.; Merényi, G.; Neta, P.; Ruscic, B.; Stanbury, D.M.; Steenken, S.; Wardman, P. Standard Electrode Potentials Involving Radicals in Aqueous Solution: Inorganic Radicals. *BioInorganic React. Mech.* **2013**, *9*, 59–61. [CrossRef]
7. Kefeni, K.K.; Msagati, T.A.M.; Mamba, B.B. Acid mine drainage: Prevention, treatment options, and resource recovery: A review. *J. Clean. Prod.* **2017**, *151*, 475–493. [CrossRef]
8. Yuan, J.; Ding, Z.; Bi, Y.; Li, J.; Wen, S.; Bai, S. Resource Utilization of Acid Mine Drainage (AMD): A Review. *Water* **2022**, *14*, 2385. [CrossRef]
9. Masindi, V.; Foteinis, S.; Renforth, P.; Ndiritu, J.; Maree, J.P.; Tekere, M.; Chatzisymeon, E. Challenges and avenues for acid mine drainage treatment, beneficiation, and valorisation in circular economy: A review. *Ecol. Eng.* **2022**, *183*, 106740. [CrossRef]
10. Akinwekomi, V.; Maree, J.P.; Masindi, V.; Zvinowanda, C.; Osman, M.S.; Foteinis, S.; Mpenyana-Monyatsi, L.; Chatzisymeon, E. Beneficiation of acid mine drainage (AMD): A viable option for the synthesis of goethite, hematite, magnetite, and gypsum—Gearing towards a circular economy concept. *Miner. Eng.* **2020**, *148*, 106204. [CrossRef]
11. Fonseka, C.; Ryu, S.; Naidu, G.; Kandasamy, J.; Vigneswaran, S. Recovery of water and valuable metals using low pressure nanofiltration and sequential adsorption from acid mine drainage. *Environ. Technol. Innov.* **2022**, *28*, 102753. [CrossRef]
12. Menzel, K.; Barros, L.; Garcia, A.; Ruby-Figueroa, R.; Estay, H. Metal sulfide precipitation coupled with membrane filtration process for recovering copper from acid mine drainage. *Sep. Purif. Technol.* **2021**, *270*, 118721. [CrossRef]
13. León, R.; Macias, F.; Canovas, C.R.; Perez-Lopez, R.; Ayora, C.; Nieto, J.M.; Olias, M. Mine waters as a secondary source of rare earth elements worldwide: The case of the Iberian Pyrite Belt. *J. Geochem. Explor.* **2021**, *224*, 106742. [CrossRef]
14. Bahmani, P.; Maleki, A.; Ghahramani, E.; Rashidi, A. Decolorization of the dye reactive black 5 using Fenton oxidation. *Afr. J. Biotechnol.* **2013**, *12*, 4115–4122.
15. Muhammad, A.; Shafeeq, A.; Butt, M.; Rizvi, Z.; Chughtai, M.; Rehman, S. Decolorization and removal of cod and bodfrom raw and biotreated textile dye bath effluent through advanced oxidation processes (AOPS). *Braz. J. Chem. Eng.* **2008**, *25*, 453–459. [CrossRef]
16. Neamtu, M.; Yediler, A.; Siminiceanu, I.; Macoveanu, M.; Kettrup, A. Decolorization of disperse red 354 azo dye in water by several oxidation processes—A comparative study. *Dye. Pigment.* **2004**, *60*, 61–68. [CrossRef]
17. Nidheesh, P.; Gandhimathi, R. Trends in electro-Fenton process for water and wastewater treatment: An overview. *Desalination* **2012**, *299*, 1–15. [CrossRef]
18. Tantak, N.P.; Chaudhari, S. Degradation of azo dyes by sequential Fenton's oxidation and aerobic biological treatment. *J. Hazard. Mater.* **2006**, *136*, 698–705. [CrossRef]
19. Lima, J.P.P.; Tabelini, C.H.B.; Aguiar, A. A Review of Gallic Acid-Mediated Fenton Processes for Degrading Emerging Pollutants and Dyes. *Molecules* **2023**, *28*, 1166. [CrossRef]
20. Klamerth, N.; Malato, S.; Maldonado, M.; Aguera, A.; Fernandez-Alba, A. Modified photo-Fenton for degradation of emerging contaminants in municipal wastewater effluents. *Catal. Today* **2011**, *161*, 241–246. [CrossRef]
21. Marcelino, R.; Queiroz, M.; Amorim, C.; Leao, M.; Brites-Nobrega, F. Solar energy for wastewater treatment: Review of international technologies and their applicability in Brazil. *Environ. Sci. Pollut. Res.* **2015**, *22*, 762–773. [CrossRef] [PubMed]
22. Tony, M.A.; Lin, L.-S. Performance of acid mine drainage sludge as an innovative catalytic oxidation source for treating vehicle-washing wastewater. *J. Dispers. Sci. Technol.* **2022**, *43*, 50–60. [CrossRef]
23. Masindi, V.; Foteinis, S.; Chatzisymeon, E. Co-treatment of acid mine drainage and municipal wastewater effluents: Emphasis on the fate and partitioning of chemical contaminants. *J. Hazard. Mater.* **2022**, *421*, 126677. [CrossRef] [PubMed]
24. Akinwekomi, V.; Maree, J.; Zvinowanda, C.; Masindi, V. Synthesis of magnetite from iron-rich mine water using sodium carbonate. *J. Environ. Chem. Eng.* **2017**, *5*, 2699–2707. [CrossRef]
25. Masindi, V.; Osman, M.S.; Mbhele, R.N.; Rikhotso, R. Fate of pollutants post treatment of acid mine drainage with basic oxygen furnace slag: Validation of experimental results with a geochemical model. *J. Clean. Prod.* **2018**, *172*, 2899–2909. [CrossRef]
26. Ali, N.S.; Kalash, K.R.; Ahmed, A.N.; Albayati, T.M. Performance of a solar photocatalysis reactor as pretreatment for wastewater via UV, UV/TiO2, and UV/H2O2 to control membrane fouling. *Sci. Rep.* **2022**, *12*, 16782. [CrossRef]

27. Dashairya, L.; Sharma, S.; Rathi, A.; Saha, P.; Basu, S. Solar-light-driven photocatalysis by Sb2S3/carbon based composites towards degradation of noxious organic pollutants. *Mater. Chem. Phys.* **2021**, *273*, 125120. [CrossRef]

28. Mancuso, A.; Morante, N.; De Carluccio, M.; Sacco, O.; Rizzo, L.; Fontana, M.; Esposito, S.; Vaiano, V.; Sannino, D. Solar driven photocatalysis using iron and chromium doped TiO_2 coupled to moving bed biofilm process for olive mill wastewater treatment. *Chem. Eng. J.* **2022**, *450*, 138107. [CrossRef]